analytical chemistry

Article

pubs.acs.org/ac

Fluorescence Quenching of Carbon Nitride Nanosheet through Its Interaction with DNA for Versatile Fluorescence Sensing

Quanbo Wang,[†] Wei Wang,[‡] Jianping Lei,[†] Nan Xu,[†] Fenglei Gao,[†] and Huangxian Ju*[,†]

[†]State Key Laboratory of Analytical Chemistry for Life Science, School of Chemistry and Chemical Engineering, Nanjing University, Nanjing, Jiangsu 210093, P.R. China

[‡]Institute of Basic Medicine, Shandong Academy of Medical Sciences, Jinan, Shandong 250062, P.R. China

Supporting Information

ABSTRACT: This work investigates the interaction of carbon nitride nanosheet (CNNS), a recently developed two-dimensional nanomaterial, with DNA and its fluorescence quenching mechanism on fluorophore labeled single-stranded DNA probes. The static quenching through the photoinduced electron transfer (PET) from the excited fluorophore to the conductive band of CNNS is identified. Utilizing the affinity change of CNNS to DNA probes upon their recognition to targets and the PET-based fluorescence quenching effect, a universal sensing strategy is proposed for design of several homogeneous fluorescence detection methods with short assay time and high sensitivity. This strategy is versatile and can be combined with different amplification tools for quick fluorescence sensing of DNA and extensive DNA related analytes such as metal cations, small molecules, and proteins. As examples, two simple fluorescence detection methods for DNA and Hg^{2+}, one facile detection method coupled with Exo III-mediated target recycling for sensitive DNA analysis, and a ratiometric fluorescence protocol for DNA detection are proposed. This work provides an avenue for understanding the interaction between two-dimensional nanomaterials and biomolecules and designing novel sensing strategies for extending the applications of nanomaterials in bioanalysis.

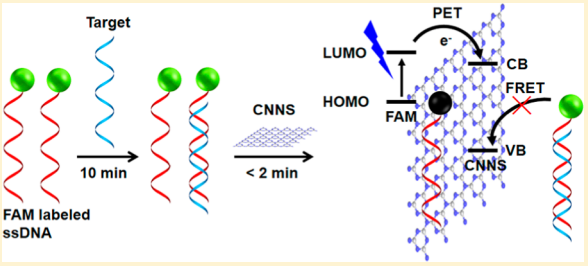

As a conceptually new class of nanomaterials, two-dimensional inorganic graphene analogues (IGAs) such as layered hexagonal boron nitride (h-BN), transition metal dichalcogenides, and transition metal oxides, which involve van der Waals interaction among adjacent layers and covalent bonding within an individual layer, have been considered to be an emerging area in nanoscience. Owing to the exotic electronic properties and high percentage of surface atoms, IGAs have shown various applications in catalysis, energy storage, optoelectronics, and sensing.[1−8] The interactions between IGAs nanosheets and biomolecules have attracted considerable attention for the potential applications in nanotechnology and bioanalysis. For example, the strong affinity of h-BN nanosheets toward ferritin implies the applications in electronics and biology,[6] and silver nanoparticle-decorated hexagonal boron nitride nanosheet has been used as thermal oxidation-resistant surface enhanced Raman substrate for detection of rhodamine 6G.[7] The stronger affinity of molybdenum disulfide nanosheets toward single-stranded DNA (ssDNA) than double-stranded DNA (dsDNA) has been used for assay of DNA and adenosine with good analytical performance.[8] Thus, it is significant to further explore new materials with high dispersity in water for design of novel sensing strategy.

Bulk graphitic-phase carbon nitride (g-C_3N_4), as a representative layered material, has been used in photochemical or electrochemical catalysis[9−11] and, lately, as probe for electrochemiluminescent, fluorescent, electrochemical, and colorimetric detection of small molecules such as Cu^{2+} and H_2O_2.[12−16] For example, the electrogenerated chemiluminescence behavior of g-C_3N_4 with $K_2S_2O_8$ as the coreactant has been employed to fabricate an electrochemiluminescent sensor for Cu^{2+} determination with high selectivity.[12] The g-C_3N_4 modified glassy carbon electrode has been used as a highly sensitive electrochemical sensor for simultaneous electrochemical detection of Pb^{2+}, Cu^{2+}, and Hg^{2+}.[15] Recently, carbon nitride nanosheet (CNNS) has been exfoliated from bulk g-C_3N_4 and used as a promising signal tag for the labeling of the membranes of HeLa cells due to its excellent biocompatibility and intrinsic blue fluorescence emission under UV-light irradiation.[17] The intrinsic blue fluorescence emission of CNNS has also been used for the fluorescent detection of Cu^{2+}.[18] To utilize the affinity of CNNS to biomolecules for extensive sensing application, this work systematically investigated its interaction with DNA. On the basis of its fluorescence quenching ability and the stronger affinity to ssDNA than dsDNA, a universal sensing strategy was proposed to design a series of homogeneous methods for fast homogeneous fluorescence detection of DNA and related analytes (Scheme 1).

Received: November 11, 2013
Accepted: November 25, 2013
Published: November 25, 2013

Scheme 1. Schematic Illustration of Interaction of DNA with CNNS, Fluorescence Quenching Mechanism of CNNS, and Sensing Strategy for Fluorescence Detection of (a) DNA and (b) Hg^{2+} and (c) Ratiometric Fluorescence Detection of DNA

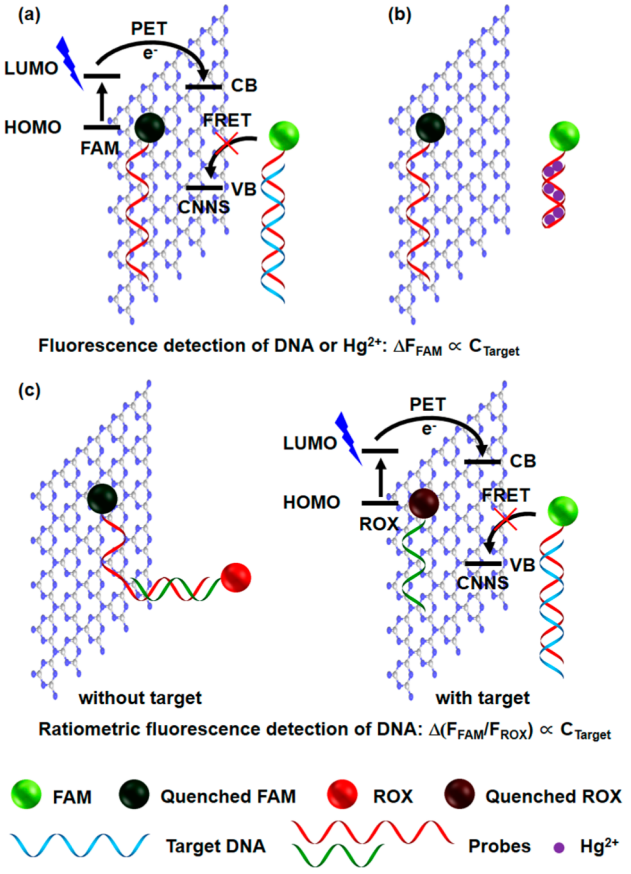

The strong interaction of CNNS with DNA can quench the fluorescence of fluorophore labeled to DNA via a static quenching approach. Upon the formation of dsDNA by hybridization of the probe with target DNA or intramolecular double helical structure by the specific recognition of bases to target analyte, the quenching efficiency (QE) is weakened, leading to an increasing fluorescence intensity (FL intensity) for the detection of DNA or Hg^{2+} (Scheme 2a,d). By introducing an Exo III-mediated target recycling for signal amplification, the fluorescence increase can be further enhanced, which produces a more sensitive method for DNA detection (Scheme 2b). In particular, the fluorescence quenching effect of CNNS through short-range photoinduced electron transfer (PET) can be used for design of a ratiometric fluorescence protocol with two complementary probes labeled with different fluorophores (Scheme 2c), which further improves the detection sensitivity of DNA. These novel sensing strategies demonstrated the fluorescence quenching effect of CNNS, and its affinity to biomolecules could be conveniently combined with recognition pairs for development of nanobiosensing platform with excellent practicability.

EXPERIMENTAL SECTION

Materials and Reagents. The oligonucleotides as well as fluorescein (FAM) or X-rhodamine (ROX) labeled DNA were synthesized and purified by TAKARA Biotechnology (Dalian,

Scheme 2. Schematic Illustration of Fluorescence Detection of DNA (a) without or (b) with Exo III-Catalyzed Cycle, (c) Ratiometric Fluorescence Detection of DNA, and (d) Fluorescence Detection of Hg^{2+} through the Quenching Effect of CNNS

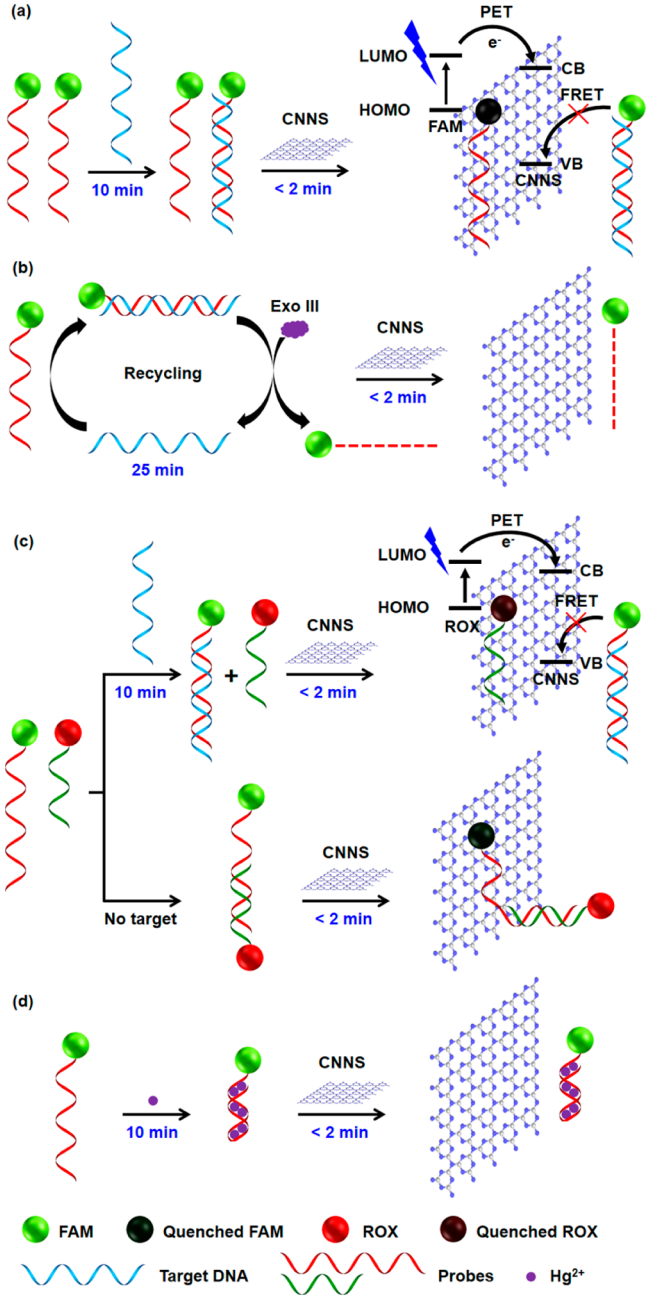

China) and Sangon Inc. (Shanghai, China). Their sequences were shown in Table S1, Supporting Information. Graphene oxide (GO) was obtained from XFNano Materials Tech Co., Ltd. (Nanjing, China). Melamine was obtained from Sigma–Aldrich Inc. (USA). Mercuric acetate and other inorganic metal salts were obtained from Sinopharm Chemical Reagent Co., Ltd. (Shanghai, China). All other reagents were of analytical grade and used without further purification. Tris–HCl buffer 1 (20 mM, containing 100 mM NaCl, 5.0 mM KCl, and 5.0 mM $MgCl_2$, pH 7.4) was used to study the interaction between CNNS and DNA, as well as homogeneous fluorescence detection of DNA without the Exo III-catalyzed cycle. Tris–

dx.doi.org/10.1021/ac403646n | Anal. Chem. 2013, 85, 12182–12188

HCl buffer 2 (20 mM, containing 5.0 mM $MgCl_2$, pH 7.4) was used for homogeneous fluorescence detection of DNA with the Exo III-catalyzed cycle. Tris−HCl buffer 3 (20 mM, containing 100 mM NaCl and 5.0 mM KCl, pH 7.4) was used for homogeneous fluorescence detection of Hg^{2+}. Ultrapure water obtained from a Millipore water purification system (≥18 MΩ cm, Milli-Q, Millipore) was used in all experiments.

Apparatus. An X-ray diffraction (XRD) pattern was recorded on a D8 Advance X-ray diffractometer (Bruker, Germany) using Cu Kα radiation (λ = 1.5418 Å). An X-ray photoelectron spectroscopic (XPS) measurement was performed using an ESCALAB 250 spectrometer (Thermo-VG Scientific, USA) with an ultrahigh vacuum generator. An transmission electron micrograph (TEM) was obtained using a JEM-2100 TEM instrument (JEOL, Japan). A tapping mode atomic force microscopic (AFM) image was acquired on an Agilent 5500 AFM/SPM system (Agilent, USA) by directly casting sample dispersion onto mica sheet. Zeta potential analysis was performed on a Zetasizer (Nano-Z, Malvern, UK). UV−vis absorption spectra were obtained with a UV-3600 UV−vis-NIR spectrophotometer (Shimadzu, Japan).

Fluorescence anisotropy was measured with a F900 fluorescence spectrometer (Edinburgh Instruments Ltd., U.K.) after mixing fluorophore labeled DNA with CNNS for 2 min. Fluorescence spectra were recorded on a RF-5301PC spectrofluorometer (Shimadzu, Japan) equipped with a xenon lamp. The fluorescence emission spectra of FAM and ROX were recorded at the excitation wavelengths of 480 and 570 nm, respectively. The synchronous scanning fluorescence spectra were recorded for ratiometric fluorescence detection of DNA at the wavelength difference ($\Delta\lambda$) of 22 nm for the simultaneous excitation of both FAM and ROX.[19]

Preparation of CNNS. CNNS was prepared by sonicating bulk graphitic-phase carbon nitride (g-C_3N_4) in water, which was first synthesized by polymerization of melamine according to literature.[17] Its concentration was estimated to be 150 μg mL^{-1}.

Homogenous Fluorescence Detection of DNA. The fluorescent probe (P3, 10 nM) in 20 mM Tris−HCl buffer 1 was mixed with different concentrations of target (T3) and incubated at 37 °C for 10 min. After CNNS (15 μg mL^{-1}) was added for 2 min, the fluorescence spectrum was measured (Scheme 2a).

The Exo III-catalyzed cycle was performed for signal amplification by adding 50 U Exo III in the mixture of fluorescent probe (P3, 10 nM) in 20 mM Tris−HCl buffer 2 and different concentrations of target (T3). After the mixture was incubated at 37 °C for 25 min and then 75 °C for 3 min to terminate the Exo III reaction, 130 μL of Tris−HCl buffer 1 and 20 μL of CNNS dispersion (150 μg mL^{-1}) were added in 50 μL of the reaction mixture for 2 min to record the fluorescence spectrum (Scheme 2b).

Ratiometric Fluorescence Detection of DNA. The fluorescent probes (P4 and P5, 10 nM) in 20 mM Tris−HCl buffer 1 were mixed with different concentrations of target (T4) and incubated at 37 °C for 10 min. CNNS (11.2 μg mL^{-1}) was then added for 2 min, and synchronous scanning fluorescence was used to record the fluorescence intensities of both FAM and ROX in a single measurement. The ratiometric fluorescence of FAM to ROX was used for the quantification of DNA (Scheme 2c).

Fluorescence Detection of Hg^{2+}. The fluorescent probe (P6, 10 nM) in 20 mM Tris−HCl buffer 3 was mixed with different concentrations of Hg^{2+}. After the mixture was incubated at 37 °C for 10 min, CNNS (15 μg mL^{-1}) was added for 2 min to record the fluorescence spectrum (Scheme 2d).

RESULTS AND DISCUSSION

Characterization of CNNS. The synthesized bulk g-C_3N_4 was demonstrated with its X-ray diffraction pattern that showed two peaks at 13.1 and 27.7 degrees (Figure S1a, Supporting Information). By exfoliating the bulk g-C_3N_4 with sonication in water, the produced CNNS showed two main peaks of carbon and nitrogen elements on the X-ray photoelectron spectrum (Figure S1b, Supporting Information). The ratio of nitrogen to carbon was calculated to be 1.36, which was close to the theoretical value of 1.33, indicating its high purity. The minor oxygen peak could be attributed to the adsorption of oxygen on CNNS. The atomic force micrograph (AFM, Figure 1a) and transmission electron micrograph (TEM, Figure 1b) of CNNS clearly showed its planar structure with a dimension of around 150 nm and a height of around 1.8 nm. Moreover, CNNS could be well dispersed in water without precipitation for several weeks due to the relatively electronegative zeta potential of −28.5 mV (Figure S2, Supporting Information).

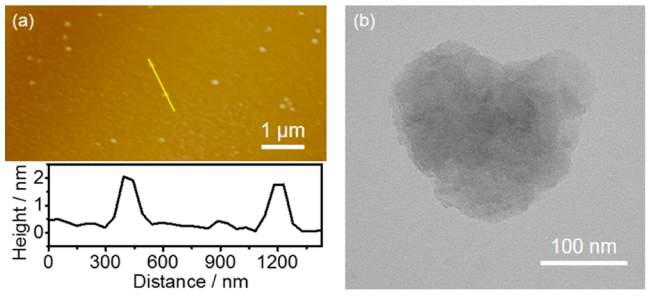

Figure 1. (a) AFM and (b) TEM images of as-exfoliated CNNS.

Owing to the large band gap of 2.70 eV,[17] CNNS did not show obvious absorption in the visible light region (Figure S3a, Supporting Information), corresponding to its colorless water dispersion (Figure S3b, Supporting Information). This large band gap leads to the intrinsic fluorescence emission of CNNS at shorter wavelength, which can be excited only at UV wavelength and thus eliminates the interference with the fluorescence measurement of fluorophores. In contrast, the UV−visible spectrum of GO showed light absorption in both ultraviolet and visible regions, corresponding to the brown appearance of its water dispersion. Besides, the CNNS dispersion showed a stronger Tyndall effect than that of GO (Figure S3b, Supporting Information), indicating its excellent stability. The good dispersity was favorable for investigation of its interaction with biomolecules and its application in the biosensing field.

Fluorescence Quenching Property and Mechanism of CNNS. The fluorescence quenching ability of CNNS was investigated with the fluorophore labeled ssDNA. Upon addition of CNNS into the solution of fluorescein (FAM) or X-rhodamine (ROX) labeled ssDNA (P1 or P2), the FL intensity greatly decreased (Figure 2a). The QE of CNNS on the fluorescence of FAM and ROX was 82.5 ± 0.5% and 77.6 ± 1.1%, respectively. Moreover, the FL intensity could reached the steady value within only 2 min (Figure 2b), indicating the fast quenching kinetics of CNNS toward both P1 and P2.

dx.doi.org/10.1021/ac403646n | Anal. Chem. 2013, 85, 12182−12188

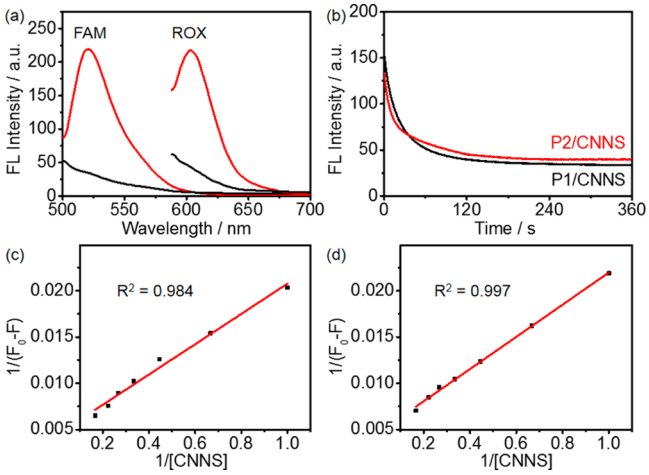

Figure 2. (a) Fluorescence spectra of 10 nM P1 (left) and P2 (right) in the absence (red) and presence (black) of 15 μg mL^{-1} CNNS. (b) Fluorescence kinetic curves of 10 nM P1 (black) and P2 (red) upon addition of 15 μg mL^{-1} CNNS. Lineweaver–Burk plots for 10 nM (c) P1 and (d) P2. F_0 and F are the FL intensity of fluorophore in the absence and presence of CNNS, respectively.

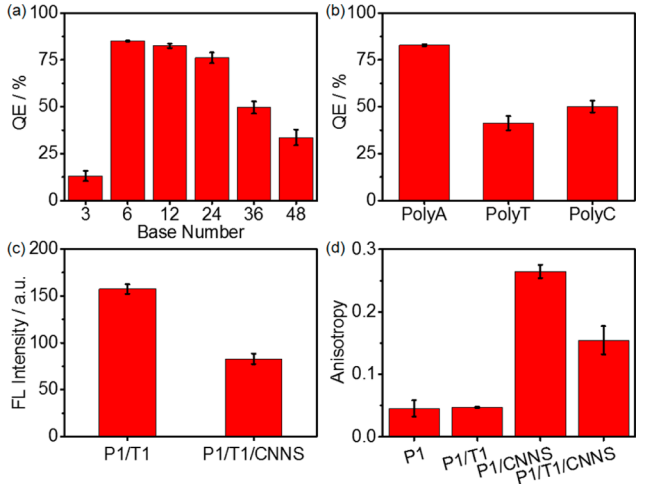

Figure 3. Dependence of QE of CNNS on (a) length and (b) nucleotide base of ssDNA. (c) FL intensities of P1/T1 before and after addition of CNNS. (d) Fluorescence anisotropy of P1, P1/T1, P1/CNNS, and P1/T1/CNNS. The concentrations of ssDNA probes, T1, and CNNS were 10 nM, 10 nM, and 15 μg mL^{-1}, respectively.

The UV–visible absorption spectra of P1 and P2 showed an absorption peak at 494 nm for FAM and 587 nm for ROX, respectively. Upon addition of CNNS, both the absorption peaks showed remarkable hypochromicity (Figure S4a,b, Supporting Information), suggesting a static interaction between CNNS and the fluorophores, which led to a close contact of the fluorophores with the conjugated plane of CNNS through π–π interaction to produce a notable electronic communication between fluorophores and CNNS.[20] The electronic communication resulted in the fluorescence quenching of FAM and ROX by CNNS. With the increasing CNNS concentration, the change of FL intensity for both P1 and P2 showed a Lineweaver–Burk plot (Figure 2c,d), while the Stern–Volmer plot showed a poor correlation (Figure S4c,d, Supporting Information). Thus, the fluorescence quenching followed the static quenching rather than the dynamic quenching mechanism.[21] From the slopes of the Lineweaver–Burk plots, the static quenching constants of CNNS toward P1 and P2 were calculated to be 3.44 ± 0.18 and 3.62 ± 0.07 μg mL^{-1}, respectively. Considering the fact that CNNS had no obvious absorption in the visible light region (Figure S3a, Supporting Information), the fluorescence resonance energy transfer (FRET) from excited fluorophore to CNNS could be excluded.[20] Thus, it could be concluded that the fluorescence quenching was due to the transfer of the photoexcited electrons from fluorophore to the conductive band of CNNS with a PET mechanism (Scheme 1).[22,23]

Both the interaction ability of CNNS with ssDNA and the quenching kinetics of CNNS on the fluorescence of fluorophore depended on the length of oligonucleotide (Figure 3a and Figure S5, Supporting Information). Due to the weak interaction of CNNS with 3-mer oligonucleotide, the QE was the lowest. However, after the probe was longer than 12 mer, the QE showed a statistically significant decrease with the increasing probe length, which possibly resulted from the easier departure of fluorophore from the CNNS due to the higher freedom and flexibility of oligonucleotide with longer strand. This property also led to the slower quenching kinetics of CNNS on the longer probe.

The base composition of ssDNA also affected the QE of CNNS. Due to the instability of ssDNA with sole consecutive guanines,[24] only the ssDNA with sole consecutive adenines, thymines, and cytosines (defined as PolyA, PolyT, and PolyC) were examined (Figure 3b). They showed the QE of 82.8 ± 0.5%, 41.2 ± 3.8%, and 50.2 ± 3.1%, respectively, indicating the affinity order of CNNS followed PolyA > PolyC ≈ PolyT. The high affinity of CNNS to PolyA was due to the stronger π–π interaction of adenine with CNNS.

After P1 hybridized with the complementary target DNA (T1) to form P1/T1 hybrid, the fluorescence QE of CNNS decreased from 82.5 ± 0.5% for P1 to 47.3% ± 3.6% (Figure 3c). This change could be attributed to the weaker interaction or affinity of CNNS to dsDNA than ssDNA due to the rigid duplex structure and the shield of phosphate backbone on the nucleotide bases, which weakened the π–π interaction between nucleotide bases and CNNS plane. The affinity difference of CNNS toward ssDNA and dsDNA was further demonstrated by the fluorescence anisotropy. The anisotropies of both P1 and P1/T1 were 0.05, while the anisotropy of P1/CNNS was greater than that of P1/T1/CNNS (Figure 3d). The 5.2-times increase in P1 anisotropy upon addition of CNNS revealed the strong π–π interaction of CNNS with ssDNA. The different affinities of CNNS toward ssDNA and dsDNA offered great opportunities for CNNS application in homogeneous fluorescence sensing of DNA and related analytes.

Fluorescence Detection of DNA without or with Exo III-Catalyzed Cycle. First, a DNA sensing protocol was designed by measuring the FL intensity increment of FAM labeled ssDNA (P3) in the presence of CNNS after being mixed with its complementary target (T3) (Scheme 2a). As shown in Figure 4a, the FL intensity increased with the increasing T3 concentration, and the plot of FL intensity increment vs. T3 concentration showed a linear relationship in the concentration range from 3.0 to 30 nM (R = 0.996). The detection limit was estimated at 3σ to be 2.1 nM.

The CNNS-based fluorescence sensing protocol could be further combined with different signal amplification strategies for improving its sensitivity. As a proof-of-concept experiment, Exo III-mediated target recycling, which has been used in

dx.doi.org/10.1021/ac403646n | Anal. Chem. 2013, 85, 12182–12188

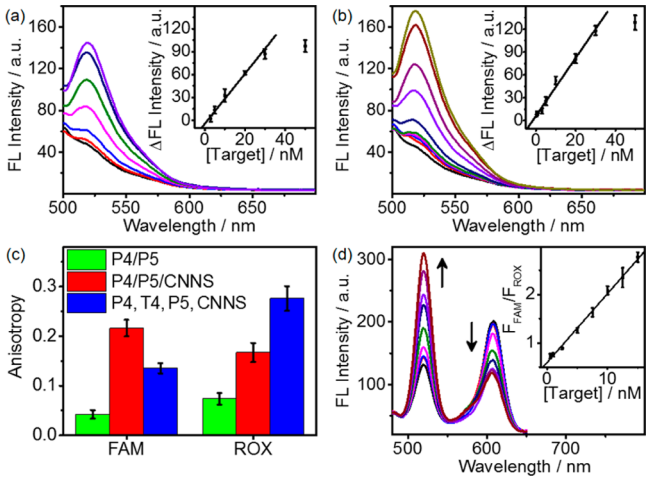

Figure 4. Fluorescence spectra of 10 nM P3 after reaction with (a) 0, 3.0, 5.0, 10, 20, 30, and 50 nM T3 (from bottom to top) for 10 min and then 15 μg mL^{-1} CNNS for 2 min and (b) 0, 0.2, 0.5, 1.0, 3.0, 5.0, 10, 20, 30, and 50 nM T3 (from bottom to top) in the presence of 50 U Exo III for 25 min and then 15 μg mL^{-1} CNNS for 2 min. Insets in (a) and (b): Calibration curve for T3 detection. (c) Fluorescence anisotropy of P4/P5 hybrid, P4/P5/CNNS, and the mixture of P4, T4, P5, and CNNS at 10 nM P4, P5, and T4 and 11.2 μg mL^{-1} CNNS. (d) Synchronous scanning fluorescence spectra of 10 nM P4 (FAM, left) and P5 (ROX, right) after reaction with 0, 0.5, 1.0, 2.5, 5.0, 7.5, 10, 12.5, and 15 nM T4 for 10 min and then 11.2 μg mL^{-1} CNNS for 2 min. Inset in (d): Calibration curve for T4 detection.

fluorescent,[25,26] electrochemical,[27,28] or colorimetric[29] detection of DNA and DNA related analytes, was introduced for signal amplification (Scheme 2b). Exo III could recognize the 3′ end of dsDNA to catalyze the hydrolysis of P3 in P3/T3 duplex, which led to the release of FAM and T3 to hybridize with another P3. The released FAM could hardly adsorb on the plane of CNNS, thus increasing the FL intensity (Figure S6, Supporting Information). The reaction time for the target recycling was optimized to be 25 min (Figure S7, Supporting Information). At the optimized reaction time, the FL intensity increment was proportional to T3 concentration ranging from 0.2 to 30 nM (R = 0.995) (Figure 4b). The detection limit was estimated at 3σ to be 81 pM, which was 26 times lower than that in the absence of Exo III. With the signal amplification step, the whole assay could be completed within 30 min.

Ratiometric Fluorescence Detection of DNA. Different from the fluorescence quenching effect of GO, which follows both long-range energy transfer and short-range electron transfer,[30−38] the fluorescence quenching effect of CNNS on both FAM and ROX via PET strongly depended on the distance between fluorophore and CNNS. Thus, a ratiometric fluorescence strategy could be designed for DNA detection. Different from the FRET-based ratiometric fluorescence methods,[39−43] this strategy used two complementary probes with different lengths (P4 and P5) which were labeled with FAM and ROX, respectively (Scheme 2c). In the absence of target DNA (T4), although the two probes could hybridize to form a duplex structure, the longer probe with FAM label (P4) could adsorb on CNNS, which led to the fluorescence quenching of FAM by CNNS. The formation of duplex structure recovered the fluorescence of ROX, producing a low fluorescence ratio of FAM to ROX. Upon addition of target DNA (T4) with longer sequence than P5, P5 was displaced by T4 to form P4/T4 hybrid. Thus, P5 was adsorbed on CNNS to quench the fluorescence of ROX, while the formed P4/T4 hybrid departed from CNNS, which recovered the fluorescence of FAM and produced a high fluorescence ratio of FAM to ROX.

The substitution of P5 by T4 or the formation of P4/T4 hybrid in the presence of P5 was identified by fluorescence anisotropy. In the presence of CNNS, the mixture of P4 and P5 showed a greater increase of FAM anisotropy than ROX anisotropy due to the adsorption of the FAM labeled single-stranded end on CNNS and the departure of the ROX labeled double-stranded end from CNNS. Upon addition of target into the mixture of P4, P5, and CNNS, the anisotropy of FAM became smaller, while the anisotropy of ROX became larger (Figure 4c), indicating the adsorption of P5 on CNNS and the departure of P4 due to the formation of P4/T4 hybrid.

The synchronous scanning fluorescence spectrum showed the opposite change of fluorescence signals from FAM and ROX with the increasing target concentration (Figure 4d). The plot of the FL intensity ratio of FAM to ROX vs. target concentration showed a linear relationship in the concentration range from 0.5 to 15 nM (R = 0.998). Although the detection limit of 0.2 nM at 3σ was slightly higher than that of 81 pM with signal amplification, the shorter assay time (12 min) and the detection limit 10-times lower than the fluorescence detection without signal amplification showed the advantages of the ratiometric fluorescence detection strategy. The specificity of both the Exo III-mediated signal amplification and the ratiometric assay was demonstrated to be acceptable for discriminating the single- and three-base mismatched DNA from the complementary target (Figure S8, Supporting Information). Compared with other nanomaterials used for homogeneous fluorescence detection of DNA, CNNS shows shorter assay time and a lower or at least comparable detection limit (Table S2, Supporting Information).

Fluorescence Detection of Hg^{2+}. Since ssDNA can be used as specific probes to recognize many other kinds of analytes such as RNA, proteins, small molecules, or metal ions, the different affinity of CNNS to ssDNA and its composite could be utilized as a universal platform for sensing DNA related analytes. Typically, a T-rich ssDNA probe (P6) was designed for the detection of Hg^{2+} based on its specific interaction with P6 (Scheme 2d). In the absence of Hg^{2+}, P6 was adsorbed onto the CNNS plane and its fluorescence was quenched. Upon the addition of Hg^{2+}, P6 recognized Hg^{2+} to form an intramolecular double helical structure via the strong affinity of T−Hg^{2+}−T base pairs,[42,44−46] which weakened the adsorption of P6 on CNNS plane and recovered its fluorescence. The FL intensity linearly increased with the increasing Hg^{2+} concentration in the range from 0.1 to 10 μM (R = 0.997) (Figure 5a). The detection limit was estimated to be 16 nM at 3σ, which was lower than the toxicity level of Hg^{2+} in drinking water (30 nM) defined by World Health Organization.[44] The CNNS-based protocol showed shorter assay time and comparable detection limit compared with previously reported fluorescence methods for Hg^{2+} detection (Table S3, Supporting Information). In addition, 10-fold concentrations of other metal cations such as Ba^{2+}, Ca^{2+}, Co^{2+}, Cu^{2+}, Mg^{2+}, Mn^{2+}, Ni^{2+}, or Zn^{2+} showed much lower FL intensity increment than Hg^{2+} (Figure 5b), indicating the excellent selectivity for Hg^{2+} detection.

dx.doi.org/10.1021/ac403646n | Anal. Chem. 2013, 85, 12182−12188

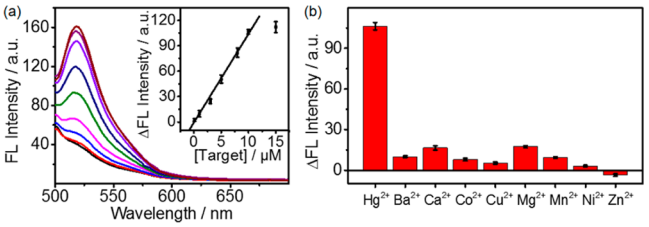

Figure 5. (a) Fluorescence spectra of 10 nM P6 after reaction with 0, 0.1, 1.0, 3.0, 5.0, 8.0, 10, and 15 μM Hg^{2+} (from bottom to top) for 10 min and then 15 μg mL^{-1} CNNS for 2 min. Inset in (a): Calibration curve for Hg^{2+} detection. (b) Fluorescence intensity increment of 10 nM P6 after reaction with 10 μM Hg^{2+} or 100 μM other metal cations for 10 min and then 15 μg mL^{-1} CNNS for 2 min.

CONCLUSIONS

CNNS as a recently developed two-dimensional nanomaterial provides a powerful platform for extensive nanobioanalysis through its interaction with DNA. The interaction leads to a strong fluorescence quenching effect of CNNS on fluorophore labeled to ssDNA with fast quenching kinetics. The quenching effect is identified to follow a static quenching mechanism through PET. On the basis of the affinity change of CNNS toward DNA probes upon the specific recognition of the probes to target analytes, the quenching effect has been utilized to design a universal sensing strategy for development of novel homogeneous fluorescence sensing methods. These methods indicate the extensible sensing application of CNNS and can be conveniently combined with signal amplification steps for further improving the sensitivity. Especially, a ratiometric fluorescence protocol is also proposed for DNA detection. Overall, this work provides an avenue for understanding the interaction between two-dimensional nanomaterials and biomolecules and extends their applications in nanobioanalysis of DNA and extensive DNA related analytes such as metal cations, small molecules, and proteins.

ASSOCIATED CONTENT

Supporting Information

Additional information as noted in the text. This material is available free of charge via the Internet at http://pubs.acs.org.

AUTHOR INFORMATION

Corresponding Author

*Phone/Fax: +86-25-83593593. E-mail: hxju@nju.edu.cn.

Notes

The authors declare no competing financial interest.

ACKNOWLEDGMENTS

We gratefully acknowledge National Basic Research Program (2010CB732400) and National Natural Science Foundation of China (21075060, 21135002, 21121091). We also thank Dr. D. D. Qi at University of Science and Technology Beijing for his insightful discussion.

REFERENCES

(1) Xu, M. S.; Liang, T.; Shi, M. M.; Chen, H. Z. *Chem. Rev.* **2013**, *113*, 3766−3798.
(2) Nicolosi, V.; Chhowalla, M.; Kanatzidis, M. G.; Strano, M. S.; Coleman, J. N. *Science* **2013**, *340*, 1226419.
(3) Wang, Q. H.; Kalantar-Zadeh, K.; Kis, A.; Coleman, J. N.; Strano, M. S. *Nat. Nanotechnol.* **2012**, *7*, 699−712.
(4) Ramakrishna Matte, H. S. S.; Gomathi, A.; Manna, A. K.; Late, D. J.; Datta, R.; Pati, S. K.; Rao, C. N. R. *Angew. Chem., Int. Ed.* **2010**, *49*, 4059−4062.
(5) Zeng, Z. Y.; Yin, Z. Y.; Huang, X.; Li, H.; He, Q. Y.; Lu, G.; Boey, F.; Zhang, H. *Angew. Chem., Int. Ed.* **2011**, *50*, 11093−11097.
(6) Lin, Y.; Williams, T. V.; Xu, T. B.; Cao, W.; Elsayed-Ali, H. E.; Connell, J. W. *J. Phys. Chem. C* **2011**, *115*, 2679−2685.
(7) Lin, Y.; Bunker, C. E.; Fernando, K. A. S.; Connell, J. W. *ACS Appl. Mater. Interfaces* **2012**, *4*, 1110−1117.
(8) Zhu, C. F.; Zeng, Z. Y.; Li, H.; Li, F.; Fan, C. H.; Zhang, H. *J. Am. Chem. Soc.* **2013**, *135*, 5998−6001.
(9) Wang, Y.; Wang, X. C.; Antonietti, M. *Angew. Chem., Int. Ed.* **2012**, *51*, 68−89.
(10) Sun, J. H.; Zhang, J. S.; Zhang, M. W.; Antonietti, M.; Fu, X. Z.; Wang, X. C. *Nat. Commun.* **2012**, *3*, 1139.
(11) Zheng, Y.; Jiao, Y.; Chen, J.; Liu, J.; Liang, J.; Du, A. J.; Zhang, W. M.; Zhu, Z. H.; Smith, S. C.; Jaroniec, M.; Lu, G. Q.; Qiao, S. Z. *J. Am. Chem. Soc.* **2011**, *133*, 20116−20119.
(12) Cheng, C. M.; Huang, Y.; Tian, X. Q.; Zheng, B. Z.; Li, Y.; Yuan, H. Y.; Xiao, D.; Xie, S. P.; Choi, M. M. F. *Anal. Chem.* **2012**, *84*, 4754−4759.
(13) Cheng, C. M.; Huang, Y.; Wang, J.; Zheng, B. Z.; Yuan, H. Y.; Xiao, D. *Anal. Chem.* **2013**, *85*, 2601−2605.
(14) Barman, S.; Sadhukhan, M. *J. Mater. Chem.* **2012**, *22*, 21832−21837.
(15) Sadhukhan, M.; Barman, S. *J. Mater. Chem. A* **2013**, *1*, 2752−2756.
(16) Liu, S.; Tian, J. Q.; Wang, L.; Luo, Y. L.; Sun, X. P. *RSC Adv.* **2012**, *2*, 411−413.
(17) Zhang, X. D.; Xie, X.; Wang, H.; Zhang, J. J.; Pan, B. C.; Xie, Y. *J. Am. Chem. Soc.* **2013**, *135*, 18−21.
(18) Tian, J. Q.; Liu, Q.; Asiri, A. M.; Al-Youbi, A. O.; Sun, X. P. *Anal. Chem.* **2013**, *85*, 5595−5599.
(19) Xiang, D. S.; Zhou, G. H.; Luo, M.; Ji, X. H.; He, Z. K. *Analyst* **2012**, *137*, 3787−3793.
(20) Marras, S. A. E.; Kramer, F. R.; Tyagi, S. *Nucleic Acids Res.* **2002**, *30*, No. e122.
(21) He, Y.; Wang, H. F.; Yan, X. P. *Anal. Chem.* **2008**, *80*, 3832−3837.
(22) Takanabe, K.; Kamata, K.; Wang, X.; Antonietti, M.; Kubota, J.; Domen, K. *Phys. Chem. Chem. Phys.* **2010**, *12*, 13020−13025.
(23) Wang, Y. B.; Hong, J. D.; Zhang, W.; Xu, R. *Catal. Sci. Technol.* **2013**, *3*, 1703−1711.
(24) Su, X.; Zhu, X. C.; Zhang, C.; Xiao, X. J.; Zhao, M. P. *Anal. Chem.* **2012**, *84*, 5059−5065.
(25) Zuo, X. L.; Xia, F.; Xiao, Y.; Plaxco, K. W. *J. Am. Chem. Soc.* **2010**, *132*, 1816−1818.
(26) Zhang, Z. X.; Balogh, D.; Wang, F.; Sung, S. Y.; Nechushtai, R.; Willner, I. *ACS Nano* **2013**, *7*, 8455−8468.
(27) Xuan, F.; Luo, X. T.; Hsing, I. M. *Anal. Chem.* **2012**, *84*, 5216−5220.
(28) Zhang, Z. J.; Wu, L.; Wang, J. S.; Ren, J. S.; Qu, X. G. *Chem. Commun.* **2013**, *49*, 9986−9988.
(29) Bi, S.; Li, L.; Cui, Y. Y. *Chem. Commun.* **2012**, *48*, 1018−1020.
(30) Lu, C. H.; Yang, H. H.; Zhu, C. L.; Chen, X.; Chen, G. N. *Angew. Chem., Int. Ed.* **2009**, *48*, 4785−4787.
(31) Dong, H. F.; Gao, W. C.; Yan, F.; Ji, H. X.; Ju, H. X. *Anal. Chem.* **2010**, *82*, 5511−5517.
(32) He, S. J.; Song, B.; Li, D.; Zhu, C. F.; Qi, W. P.; Wen, Y. Q.; Wang, L. H.; Song, S. P.; Fang, H. P.; Fan, C. H. *Adv. Funct. Mater.* **2010**, *20*, 453−459.
(33) Lu, C. H.; Li, J.; Lin, M. H.; Wang, Y. W.; Yang, H. H.; Chen, X.; Chen, G. N. *Angew. Chem., Int. Ed.* **2010**, *49*, 8454−8457.
(34) Chang, H. X.; Tang, L. H.; Wang, Y.; Jiang, J. H.; Li, J. H. *Anal. Chem.* **2010**, *82*, 2341−2346.
(35) Zhao, X. H.; Kong, R. M.; Zhang, X. B.; Meng, H. M.; Liu, W. N.; Tan, W. H.; Shen, G. L.; Yu, R. Q. *Anal. Chem.* **2011**, *83*, 5062−5066.

(36) Chen, L.; Zhang, X. W.; Zhou, G. H.; Xiang, X.; Ji, X. H.; Zheng, Z. H.; He, Z. K.; Wang, H. Z. *Anal. Chem.* **2012**, *84*, 3200−3207.
(37) Cui, L.; Chen, Z. R.; Zhu, Z.; Lin, X. Y.; Chen, X.; Yang, C. J. *Anal. Chem.* **2013**, *85*, 2269−2275.
(38) Mao, X. W.; Su, H. Y.; Tian, D. M.; Li, H. B.; Yang, R. H. *ACS Appl. Mater. Interfaces* **2013**, *5*, 592−597.
(39) Zhang, P.; Beck, T.; Tan, W. H. *Angew. Chem., Int. Ed.* **2001**, *40*, 402−405.
(40) Ueberfeld, J.; Walt, D. R. *Anal. Chem.* **2004**, *76*, 947−952.
(41) Jockusch, S.; Marti, A. A.; Turro, N. J.; Li, Z. M.; Li, X. X.; Ju, J. Y.; Stevens, N.; Akins, D. L. *Photochem. Photobiol. Sci.* **2006**, *5*, 493−498.
(42) Wu, J. C.; Zou, Y.; Li, C. Y.; Sicking, W.; Piantanida, I.; Yi, T.; Schmuck, C. *J. Am. Chem. Soc.* **2012**, *134*, 1958−1961.
(43) Yang, Y. B.; Ji, S. M.; Zhou, F. K.; Zhao, J. Z. *Biosens. Bioelectron.* **2009**, *24*, 3442−3447.
(44) Zhang, L. B.; Li, T.; Li, B. L.; Li, J.; Wang, E. K. *Chem. Commun.* **2010**, *46*, 1476−1478.
(45) Zhang, Y. F.; Yuan, Q.; Chen, T.; Zhang, X. B.; Chen, Y.; Tan, W. H. *Anal. Chem.* **2012**, *84*, 1956−1962.
(46) Stobiecka, M.; Molinero, A. A.; Chałupa, A.; Hepel, M. *Anal. Chem.* **2012**, *84*, 4970−4978.